




Oxide-Free Copper Pastes for the Attachment of Large-Area Power Devices

LUCA DEL CARRO ^{1,2,4} ALFRED A. ZINN,³ PATRICK RUCH,¹
FLORIAN BOUVILLE,² ANDRÉ R. STUDART,²
and THOMAS BRUNSCHWILER¹

1.—IBM Research – Zurich, Säumerstrasse 4, 8803 Rüschlikon, Switzerland. 2.—Complex Materials, Department of Materials, ETH Zürich, 8093 Zurich, Switzerland. 3.—Kuprion Inc., Palo Alto, CA 94303, USA. 4.—e-mail: luca.delcarro@gmail.com

Pastes based on copper (Cu) nanoparticles (NPs) are promising electronic-packaging materials for the attachment of high-power devices. However, the rapid oxidation of nanostructured Cu requires the use of reducing agents during processing, which makes it less suitable for attaching large-area dies ($> 4 \text{ mm}^2$). Recently, the functionalization of Cu-NP surfaces with a mixture of amines prevented oxidation, allowing for sintering without the need for reducing agents. Here we investigate the sintering mechanisms involved during die attachment using pastes of passivated Cu NPs, with particular focus on the critical role of the carrier solvents. Using 1-nonanol or 1-decanol as solvents, we first demonstrate the absence of Cu-oxide phases in the pastes after fabrication and the stability of the resulting nanostructured copper for as much as 30 min in air. By measuring the evolution of the electrical characteristics of the paste during drying and sintering, we show that electrically conductive agglomerates form among the NPs between 141°C and 144°C , independent of the carrier solvent used. The carrier solvent was found to affect mainly the densification temperature of the copper agglomerates. Because they lead to uniform sintering of the material, Cu pastes based on solvents with a low boiling point and high vapor pressure are preferable for attaching dies with area greater than 25 mm^2 . We show that dies with an area as large as 100 mm^2 can be attached using a Cu paste based on 1-nonanol. These pastes enable the formation of temperature-resistant bonding for high-power devices using a simple and cost-effective approach.

Key words: Sintering, copper nanoparticles, copper paste, die attachment, power electronic packaging, power electronics

INTRODUCTION

Direct integration of silicon-based electronic devices in systems that operate in conditions of high power and high ambient temperature has been hindered by their maximum operation temperature of 150°C , which is set in order to avoid the excessive generation of intrinsic carriers in silicon (Si).¹

Recently, wide-band-gap semiconductors such as silicon carbide (SiC) and gallium arsenide (GaAs) have been introduced to replace Si, resulting in electronic devices able to operate at temperatures beyond 300°C .^{2–4} However, these high operational temperatures are not suitable for the traditional packaging materials that are applied to connect electrically, thermally and mechanically the device to the substrate, in the so-called die attachment operation. In fact, the widely applied lead-free solders re-melt above 250°C .^{5,6} Furthermore, the high-melting solder formulations based on lead,

(Received February 16, 2019; accepted July 11, 2019; published online July 29, 2019)

bismuth or gold are not applicable on a large scale due to their environmental toxicity, low electrical conductivity or high cost, respectively.^{7,8} Therefore, a bonding material that is stable above 300°C, has high electrical and thermal conductivities, low cost, and is compatible with today's standard die-attachment process is highly demanded.

In this context, pastes based on metal nanoparticles (NPs) dispersed in a carrier solvent have become an attractive alternative. As a consequence of the high area-to-volume ratio of NPs, these materials can be applied and sintered at temperatures below 300°C. After sintering, the area-to-volume ratio of the material drops, and the material becomes stable until its melting point, which is often above 800°C. Moreover, these pastes are compatible with today's standard die attachment process, and thus do not require the introduction of dedicated tools. Among the various possible metals, silver (Ag) NP-based pastes have been largely studied for die attachment due to the high electrical and thermal conductivities and strong oxidation resistance of this precious metal.^{9,10} However, severe electromigration damage and dendritic growth have been reported for sintered Ag pastes when exposed to high current density and temperatures.¹¹ Moreover, its elevated cost has made it undesirable for up-scaling to large production volumes.⁵

To overcome these issues, the attention of the research community has turned to copper (Cu) NP-based pastes. Cu has a higher resistance to electromigration and is cheaper than Ag, while still exhibiting high electrical and thermal conductivities.¹² However, Cu NPs readily oxidize when exposed to ambient atmosphere, forming oxide shells that limit the diffusivity of the Cu atoms between the NPs in reciprocal contact. This oxide passivation raises the sintering temperature and lowers the final electrical conductivity of the sintered material, thus impeding its applicability.

Many approaches have been proposed to solve this problem, ranging from coating NPs with thermally activated reducing agents to synthesizing Cu NPs in situ via Cu-based metal-organic decomposition (MOD) during sintering.¹³⁻¹⁷ Although outstanding results have been reported for applications in printable electronics, only a few studies have focused on the specific case of die attachment. In this application, the Cu paste is squeezed between the die and the substrate in a sandwich-like structure (Fig. 1). The limited permeability of this sandwich structure limits the transport of gases during sintering of the Cu pastes, especially in large-area dies. In this case, Cu NPs are typically dispersed in a carrier solvent, and the resulting paste is directly applied to the substrate. The paste is then dried before the die is placed on the substrate and finally sintered in a hydrogen-based atmosphere in order to reduce the copper oxide that eventually forms during fabrication and handling of the NPs.¹⁸ Although this approach leads to successful

reduction of the Cu NPs, a maximal die area of only 4 mm² could be bonded due to the limited penetration of the reducing atmosphere into the sandwich-like structure. Furthermore, the drying pre-step limits the wetting of the metallization layer of the die, thus requiring a high bonding pressure during the process, which can damage the brittle SiC die.

In an innovative approach, the passivation of Cu-NPs surfaces with a mixture of amines has been recently reported to prevent oxidation.¹⁹⁻²² This amine-based coating is formed during the synthesis of the Cu NPs, acting as a physical barrier that avoids the agglomeration of the NPs and their exposure to oxygen. During sintering, the coating desorbs thermally from the surface of the NPs, leading to exceptional sintering without the need for a drying pre-step or a reducing agent. This approach can be potentially exploited to formulate Cu pastes suitable for attaching large dies (> 4 mm²).²³ Despite these promising results, successful bonding has so far only been reported for die areas of 1 mm². Furthermore, the role of the passivation layer and the carrier solvent during sintering of the Cu paste in the die attachment process has not yet been investigated. Because the passivation layer may affect the sintering temperature and limit the densification of the material within the constrained configuration of the die attachment layer, a systematic investigation of the sintering behavior of such amine-protected Cu NPs is crucial to enable their use for bonding of large-area dies.

In this work, we study the sintering behavior of Cu pastes containing amine-passivated Cu NPs dispersed in different carrier solvents, taking into account the specific constraints of the die attachment process (Fig. 1). Our primary focus is to understand the role of the different paste constituents in the sintering process in order to understand how to design paste formulations for strong bonding of large-area dies. First, we demonstrate that our paste fabrication method leads to oxide-free Cu NPs that can be sintered in inert atmosphere without the addition of a reducing agent. Second, we report on the evolution of the electrical and physical characteristics of these materials during sintering for two different carrier solvents. We also investigate the role of the passivation layer and the carrier solvent in defining the onset temperature for sintering and densification of the material. Finally, we demonstrate the applicability of the proposed paste formulations to attaching dies with an area of up to 100 mm².

EXPERIMENTAL SECTION

Materials

Copper-Nanoparticle-Based Pastes

In this work, the Cu NPs (Kuprion Inc., Palo Alto, CA, USA) were synthesized via a bottom-up

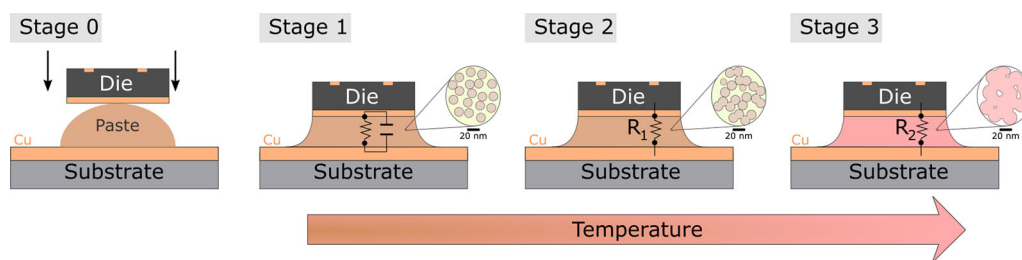
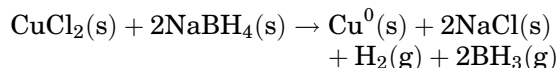


Fig. 1. Schematic representation of the sintering process of the evaluated Cu NP pastes, when applied for die attachment. Stage 0: The paste is applied to the substrate and the die is placed on top of the paste, forming a sandwich-like structure. Stage 1: At room temperature, the Cu NPs have few reciprocal contacts, resulting in a mixed capacitive and ohmic electrical behavior of the paste. Stage 2: Over a defined temperature, necks start to form between the nanoparticles, leading to percolation and consequently to an electrical connection between the substrate and the die. Stage 3: By increasing the temperature further, the materials starts to densify, thus reducing its electrical resistance.

Table I. Cu paste formulations produced with the same batch of Cu NPs

Cu paste	Carrier solvent	Solvent boiling point (°C)	Solvent vapor pressure (Pa)
Decanol	1-decanol C ₁₀ H ₂₂ O	233	1.134
Nonanol	1-nonanol C ₉ H ₂₀ O	213.3	3.026

approach in a non-aqueous glyme medium by reducing anhydrous copper(II) chloride with sodium borohydride in the presence of a mixture of amines based on Hexylamine (boiling point = 131°C) and Dihexylamine (boiling point = 195°C):²⁴



After the reduction, Cu NPs were formed with a size distribution from 10 nm to 60 nm.²⁵ These NPs were passivated by the used mixture of amines that forms an inverse micelle structure on the surface.¹⁹ Passivation was performed in order to hinder the aggregation of the NPs and to protect them from oxidation. The reaction of the amines and the borane formed stable borane-amine complexes. Subsequently, the product was washed with distilled water to remove the NaCl byproduct and to hydrolyze the borane-amine complexes into benign sodium borate (Na₂[B₄O₅(OH)₄]·8H₂O) that can be safely disposed. To the best of our knowledge, the mixture of amines cannot reduce the copper oxide.

Finally, the washed NPs were isolated by centrifugation, then a carrier solvent was added to obtain a paste with a density of 4 g/cm³ (± 0.4 g/cm³), holding a metal load of 88–89 wt.%. For this work, two paste formulations were used, containing 1-nonanol (Nonanol paste) and 1-decanol (Decanol paste) as carrier solvents (Table I).

We succeeded in scaling the manufacturing process of these Cu pastes from 50 g to 1 kg pilot plant. Currently, a scale-up to a production of 600 kg per annum is underway. This manufacturing process is protected by several patents.^{26,27}

CHARACTERIZATION TECHNIQUES

Sintering Profile

The Cu pastes were sintered in an oven (ATV Technologie, Vaterstetten, Germany) with a heating profile from 25°C to 300°C at a rate of 20 K/min and with isothermal steps of 20 s at 95–145–165–300°C. This process, referred to as the “sintering profile”, was performed in nitrogen atmosphere.

Raman Analysis

Raman spectroscopy was performed with a laser scanning confocal microscope (SCM) of Raman scattering (Spectra Raman, NT-MDT). A solid-state laser (473 nm, 50 mW, Coherent) was used as excitation source. The input and output radiation were focused and collected through the microscope objective (LPlanFL N, 100X, Olympus). The backscattered light was filtered with a neutral-density (ND) filter, which was then directed to a spectrometer (NTEGRA SPECTRA, NT-MDT) and finally to a charge-coupled device detector (Newton 920, Andor).

The samples were prepared by stencil-printing a thin film of Cu paste onto a silicon substrate with thermally grown silicon oxide (SiO₂) of 200-nm thickness. All the presented spectra were obtained at room temperature in air, with a recording time of 600 s and ND equal to 2.

Impedance Spectroscopy and Electrical Measurement

We designed and fabricated dedicated sample cells with four terminals by depositing Au electrodes

on a passivated Si substrate (Fig. 2). A sampling area of $10 \times 10 \text{ mm}^2$ was realized at the center of the cell, comprising interdigitated electrodes with a finger width of $100 \mu\text{m}$ and side-to-side separation of $50 \mu\text{m}$ (Fig. 2a).

We used optical lithography to fabricate the interdigitated electrodes by evaporating 10 nm of titanium (Ti) and 200 nm of Au on a SiO_2 (200 nm)/Si wafer. After processing, the wafer was diced to separate the cells, and Kapton-coated Cu wires were attached to the Au pads with Ag-filled epoxy (H20S, EPO-TEK). The contacted cell was placed inside the sintering oven described above to allow in situ impedance characterization during execution of the sintering profile. Prior to the impedance measurements, a small amount of Cu paste was applied to the cell and sandwiched with a glass die to reproduce the process of die attachment, while providing optical access to the paste during sintering (Fig. 2b). A detailed description of the impedance spectroscopy setup is provided in Figure S1 of the Supplementary Information.

The impedance was recorded using a potentiostat (SP-300, Bio-Logic) to apply a sinusoidal voltage input with an amplitude of 10 mV to the cell in a four-electrode configuration (Fig. 2a). The frequency was recorded from 200 kHz to 500 mHz averaging over two measurements in approximately 34 s. The measurement was continuously repeated during execution of the sintering profile. In addition, optical images of the sampling area were recorded at intervals of 1 s during the entire sintering profile (Dino-Lite 3).

The electrical resistivity of the Cu films sintered on passivated Si substrates was measured by a four-point contact probe (Jandel universal probe stand).

Thermal Analysis

Thermogravimetric analysis (TGA) and differential scanning calorimetry (DSC) were performed using a Mettler Toledo TGA 851 and a Netzsch Phoenix DSC 204, respectively. For each analysis,

about 15 mg of paste was placed in an aluminum capsule with a punched opening of 0.5 mm diameter in the lid. All measurements were performed by running a heating profile from 25°C to 300°C at a rate of 20 K/min in nitrogen atmosphere.

Die Attachment and Cross Section Preparation

Silicon dies of $10 \times 10 \text{ mm}^2$ and Si substrates of $20 \times 20 \text{ mm}^2$ were coated on one side with 10 nm of Ti and 200 nm of Cu. Then, Cu paste was applied to the Cu/Si side of the substrate and the Cu/Si side of the die was placed on top of it with a FC150 flip-chip bonder (SET, Saint Jeoire, France) at an applied load of 50 g. Finally, the assembly underwent the sintering profile, with no pressure applied on the die.

After sintering, cross sections of the assembly were prepared by chemical-mechanical polishing (CMP, Struers Tegramin 20, Denmark) and ion milling (Oxford Instruments, Ionfab 300, UK), and imaged with a scanning-electron microscope (SEM, Leo1550, Zeiss, Germany).

Microstructural Analysis and Evaluation of Macrovoids

Thin films of the Cu pastes were printed on passivated Si substrates and sintered at different maximum temperatures, held for 5 min in argon atmosphere. The size of the domains was evaluated with Fiji software by analyzing scanning-electron microscope (SEM, Leo1550, Zeiss, Germany) images of the sintered samples. Ten images were analyzed for each sintering temperature. Details of the analysis procedure and an example are given in the Supplementary Information (Supplementary Information, Figure S2 and Supplementary methods).

Electron backscatter diffraction (EBSD) was performed on cross-section samples prepared as described above and further polished by broad ion

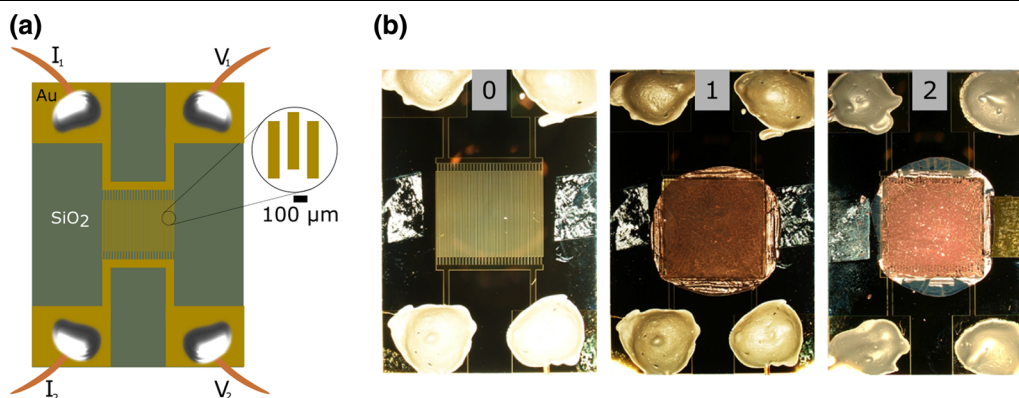


Fig. 2. (a) Schematic representation of the four-terminal cell with Au electrodes on a passivated Si substrate shown in gold and green, respectively; (b) optical images of the cell (0) after fabrication, (1) after dispensing the Cu paste and placing a glass die of $10 \times 10 \text{ mm}^2$ area, and (2) after sintering (Color figure online).

beam milling (Hitachi IM4000), using the flat milling setup with gracing incidence angle of 5° . The analysis was performed with a SEM Quanta 200F (FEI, USA) equipped with a detector Hikari (Ametek-EDAX, USA) on an area of $10 \times 10 \mu\text{m}^2$ at steps of 20 nm. The acquired data was subjected to standard cleaning procedures involving a grain tolerance angle of 5° and a minimum grain size of two pixels. Further separation between grains and pores was achieved by grain size filtering. The porosity of the sintered layer was calculated by image analysis (Fiji) on SEM images of the samples.

We calculated the percentage of voids in the sintered Cu films by analyzing (Fiji) optical images of die areas $\leq 25 \text{ mm}^2$ with a Leica DVM2500, whereas for die areas $> 25 \text{ mm}^2$ we used a Nikon SMZ1000. The different illumination sources of the two microscopes produced images with a slight color difference of the sintered material. Only voids with areas greater than $5000 \mu\text{m}^2$ were considered, which we call macrovoids. Five samples were analyzed for each set of conditions.

RESULTS AND DISCUSSION

Characterization of the Cu Pastes

The absence of copper oxide in the pristine paste is crucial for obtaining a sintered material with an electrical resistivity comparable to that of bulk Cu without the need for reducing agents. Moreover, it is important to know how long the paste can be exposed to air without oxidizing in order to evaluate its lifespan and thus to create a customized processing protocol.

The oxidation resistance of our passivated Cu nanoparticles was evaluated using four samples, which were prepared by stencil-printing a thin film of nonanol paste on passivated Si substrates. After printing, the samples were exposed to air for different durations and temperatures (Table II).

First, the samples were analyzed by Raman spectroscopy to assess the presence of copper oxide in the paste (Fig. 3a). Sample 1 was analyzed immediately after printing, where no Raman activity was observed. Sample 2 was first exposed to air at 22°C for 2 days and then measured, showing a smooth shoulder between 528 cm^{-1} and 625 cm^{-1} . Sample 3 was exposed to air under the same conditions for 10 days, which resulted in a greater intensity of the shoulder and a weak peak at 218 cm^{-1} . Finally, specimens exposed to air at 90°C for 1 h (sample 4) showed clear peaks at 150 cm^{-1} , 218 cm^{-1} , 528 cm^{-1} and 625 cm^{-1} . All the detected peaks are attributed to the vibrational modes of cuprous oxide (Cu_2O).^{28,29} The absence of Cu_2O in the pristine paste indicate that our fabrication process does not oxidize the Cu NPs. Moreover, the intensity of the Cu_2O peaks increases with the duration of air exposure, suggesting the growth of an oxide layer on the NP surface.

Table II. Samples for characterizing a pristine Nonanol paste and its lifespan when exposed to air

Sample	Conditions of air exposure
1	Analyzed immediately after printing (pristine)
2	2 days at 22°C
3	10 days at 22°C
4	1 h at 90°C

After Raman analysis, each sample was sintered at a maximum temperature of 300°C in nitrogen atmosphere. Then, their electrical resistivity ρ was measured, yielding values of $5.8 \mu\Omega \text{ cm}$, $300 \mu\Omega \text{ cm}$, $1200 \mu\Omega \text{ cm}$ and $1 \times 10^9 \mu\Omega \text{ cm}$ for Samples 1–4, respectively (Fig. 3b). The ρ value of Sample 1 is only three times that of bulk Cu, showing that this material can achieve outstanding electrical conductivity even if sintered without reducing agents. Sample 1 was sintered 30 min after printing, which, therefore, can be considered the lifespan of the nonanol-based paste. Considering that 1-decanol is less volatile and has a higher boiling point than 1-nonanol, a similar lifespan is expected for the decanol-based formulation. Furthermore, the increase of ρ as a function of the duration of air exposure confirms the increased thickness of the Cu_2O layer, which is a *p*-type semiconductor.^{30,31}

Finally, we analyzed the morphology of the sintered samples by SEM imaging (Fig. 3c). Sample 1 showed densified agglomerates formed by necking between the NPs. In Sample 2, non-densified agglomerates were observed, with the presence of dots on the surface that can be attributed to Cu_2O .¹⁴ These dots became more visible in Sample 3, with a recurrent formation of agglomerates among the NPs. In contrast, Sample 4 exhibited disconnected NPs. This analysis confirms that the complete absence of copper oxide is fundamental to activating the mechanisms of sintering of the Cu NPs at 300°C without reducing agents. This is due to the increase of the sintering temperature given by the presence of the copper oxide phase on the surface of the NPs,³² which hinders the surface diffusion of the Cu atoms. Furthermore, the lack of sintering in all the samples that contain copper oxide confirms that the amine mixture used in these experiments does not reduce Cu_2O during sintering.

Evolution of the Electrical Characteristic During Sintering

The electrical characteristic of the Cu paste is a clear indicator of the sintering level of the material, as it is affected primarily by the extent of cohesion of the Cu NPs. In the pristine state, the paste is an electrical insulator, while it becomes an electrical conductor during the sintering process. To explore this transition as a measure of the level of interconnectivity between the Cu NPs, impedance

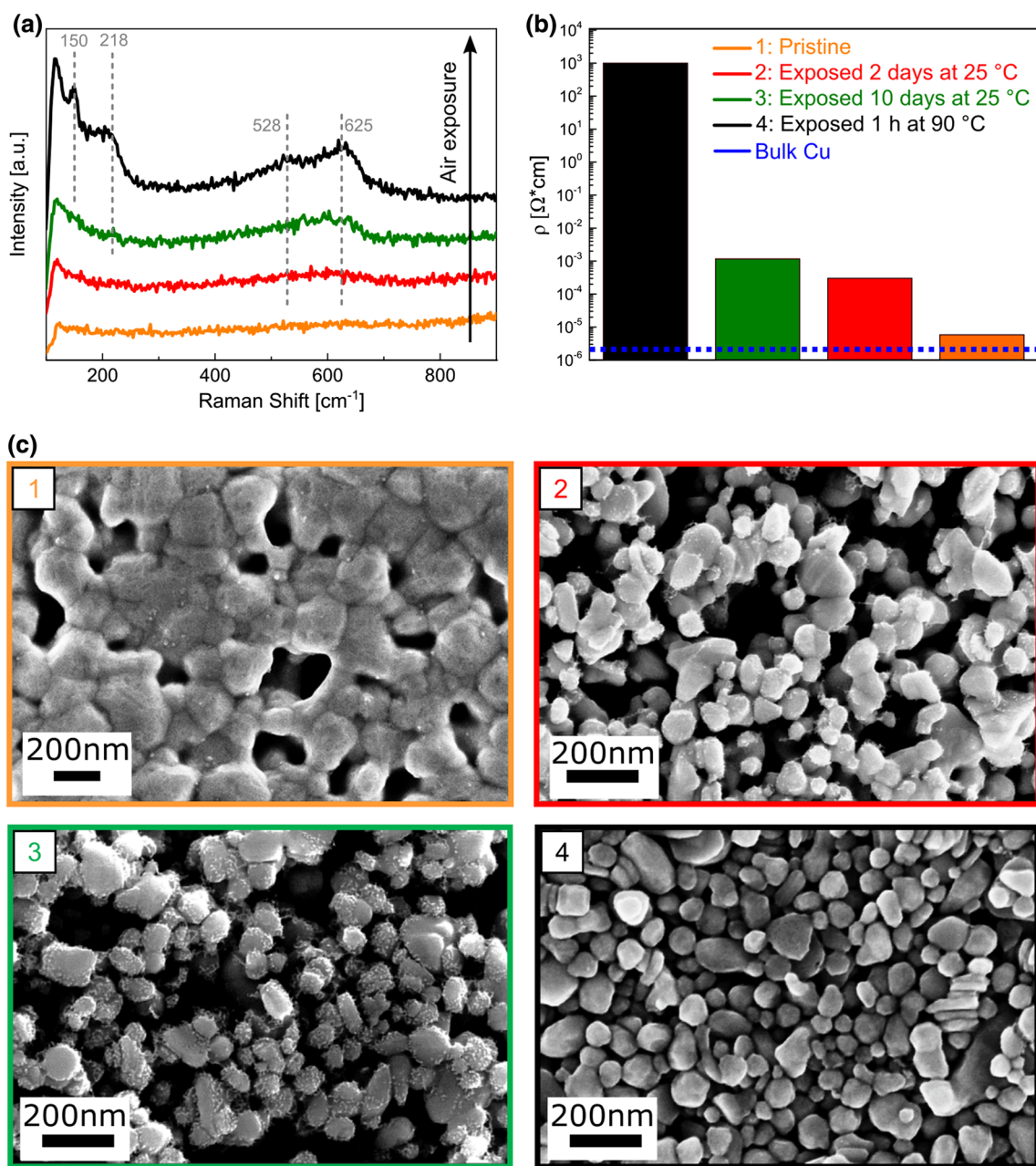


Fig. 3. Chemical, electrical and structural analysis of thin films of nonanol-based paste exposed to air for different durations. (a) Raman spectra of the investigated samples, indicating the peaks attributed to Cu_2O ; (b) Electrical resistivity of the printed samples after being sintered at a maximum temperature of 300°C in nitrogen atmosphere compared to bulk Cu; (c) Scanning electron microscope (SEM) images of the sintered samples.

spectroscopy (IS) was performed in situ on samples of decanol and nonanol-based pastes during the sintering procedure (Fig. 4).

The typical evolution of the modulus of the impedance $|Z|$ and the phase angle δ of the two mixtures during sintering are presented as Bode plots for the characteristic temperatures of 30°C , 97°C , 139°C , 144°C and 208°C (Fig. 4). These temperatures are subject to a maximum variation of $\pm 3^\circ\text{C}$ due to the duration of the impedance

measurements with respect to the heating rate. For completeness, the Nyquist representation is reported in Supplementary figure S4.

A similar evolution of the impedance was observed for both pastes during sintering. At the starting temperature of 30°C , the $|Z|$ and δ were frequency-dependent, indicative of a mixed capacitive and resistive electrical characteristic of the pastes.³³ Increasing the temperature to 97°C , a progressive decrease of $|Z|$ and $|\delta|$ at frequencies

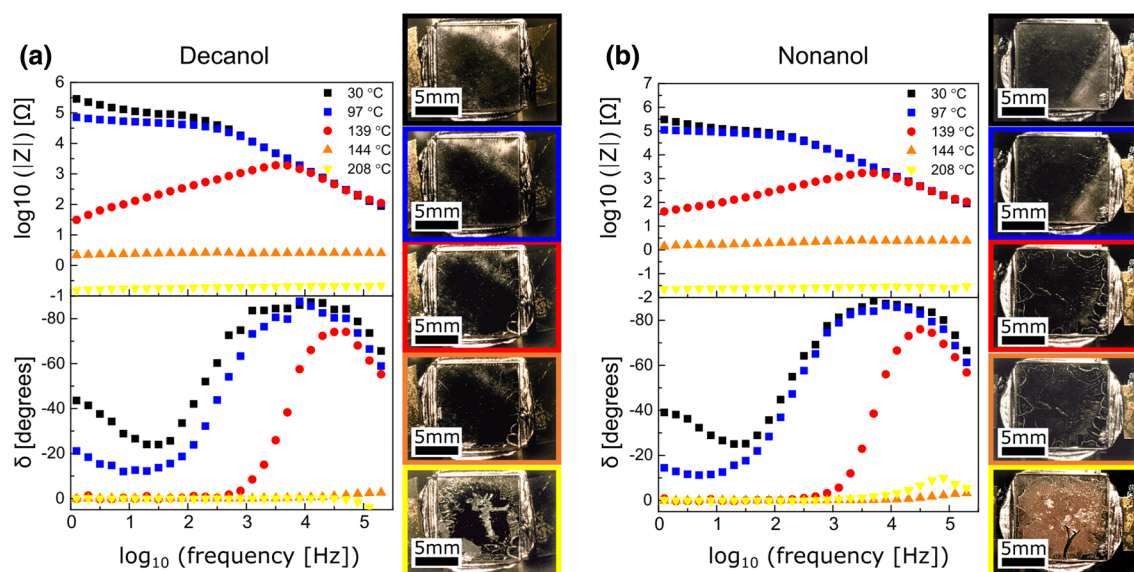


Fig. 4. Total impedance Z and impedance phase angle δ as a function of frequency for (a) decanol- and (b) nonanol-based Cu pastes. The temperature values have a maximal variation of $\pm 3^\circ\text{C}$ during the respective impedance measurement. For each curve, the corresponding optical image of the sampled area is shown.

below 1 kHz was measured, whereas these values remained almost unchanged at higher frequencies. Moreover, no significant visual variations in the paste films were observed at these temperatures. The impedance at lower frequencies can be associated with double-layer charging at the NPs surface and mass transfer resistances.³⁴ At higher frequencies, double-layer charging does not affect the impedance, and thus only the ohmic resistance of the liquid phase contributes to the measured impedance.

At approximately 139°C , a significant change of the impedance spectra occurred for both pastes as δ dropped to zero for frequencies below 1 kHz, and macrovoids started to appear in both paste films. In this frequency range, $|Z|$ decreased by approximately three orders of magnitude.

As it reached 144°C , δ levelled out to zero and the $|Z|$ value became frequency-independent for both samples in the entire frequency range studied. These changes led to the reset of the imaginary part of the impedance, indicative of a purely resistive electrical characteristic. Considering the temperature error in the measurement, this transition from frequency-dependent to frequency-independent $|Z|$ and δ values can be more precisely located in a temperature range between 141°C and 144°C .

Upon further increasing temperatures, a progressive decrease of the $|Z|$ value was observed. At 208°C , the decanol- and nonanol-based pastes exhibited a frequency-independent $|Z|$ values of 187 and 25 m Ω , respectively, at phase angles of 0° . Furthermore, the images of the decanol-containing paste showed an extensive formation of macrovoids and delamination from the glass die, whereas for the nonanol-based paste, a clear color transition from brown to orange was observed.

The reported change from a frequency-dependent to a frequency-independent system shows a transition from a mixed capacitive and resistive to a purely resistive electrical characteristic of the pastes during heat treatment. This transition indicates that, initially, the Cu NPs are electrically disconnected. However, when temperatures between 141°C and 144°C are reached, the NPs start to connect and eventually form a percolating network that bridges the interdigitated electrodes.³⁵ This network extends to length scales of at least 50 μm , which is the required minimum distance to connect the electrodes of the designed cell. Macrovoids start to form in both pastes before the onset of sintering, which is related to the high capillary forces that arise during evaporation of the solvent. These capillary forces pull the NPs together, thus promoting the formation of agglomerates and macrovoids.^{36–38} However, the process of neck formation starts in the same temperature range for both mixtures, suggesting that the onset temperature of sintering is not primarily affected by the properties of the carrier solvent. This hypothesis is supported by the similar behavior observed for two other paste formulations with mixtures of 1-decanol/octanol and dodecanol/octanol as carrier solvents (Supplementary Information, Figure S3). Despite the similar onset sintering temperatures, the differences in the $|Z|$ values and in the color of the nonanol- and decanol-containing mixtures above 200°C suggest a diverse extent of densification of the materials, which is potentially related to the different evaporation behaviors of these solvents.

The necking among the NPs observed between 141°C and 144°C is expected to occur only after the passivation layer is released from the surface of the

NPs. This should allow for the diffusion of the Cu atoms on the surface, and thus the formation of necks. To understand the role of the passivation layer, we studied the physical transformation of these materials during sintering.

Thermal Analysis During Sintering

Thermogravimetric analysis (TGA) and differential scanning calorimetry (DSC) were performed on samples of decanol- and nonanol-based pastes to evaluate the temperature at which the solvent and passivating molecules are removed during sintering (Fig. 5).

The TGA was used to record the mass changes in the samples during sintering with respect to the initial mass measured at room temperature. This analysis showed an onset of mass loss above 50°C in both samples. At 125°C, a mass reduction of 0.3% and 0.5% was recorded for the decanol- and nonanol-containing pastes, respectively. Above 125°C, the rate of mass loss increased, leading to a total mass reduction of 7.1% for the decanol paste and 8.1% for the nonanol paste at 220°C. After that, the rate of mass loss decreased for both formulations, leveling off at 300°C with a total mass reduction of 9.6% and 9.4% for the decanol and nonanol mixtures, respectively.

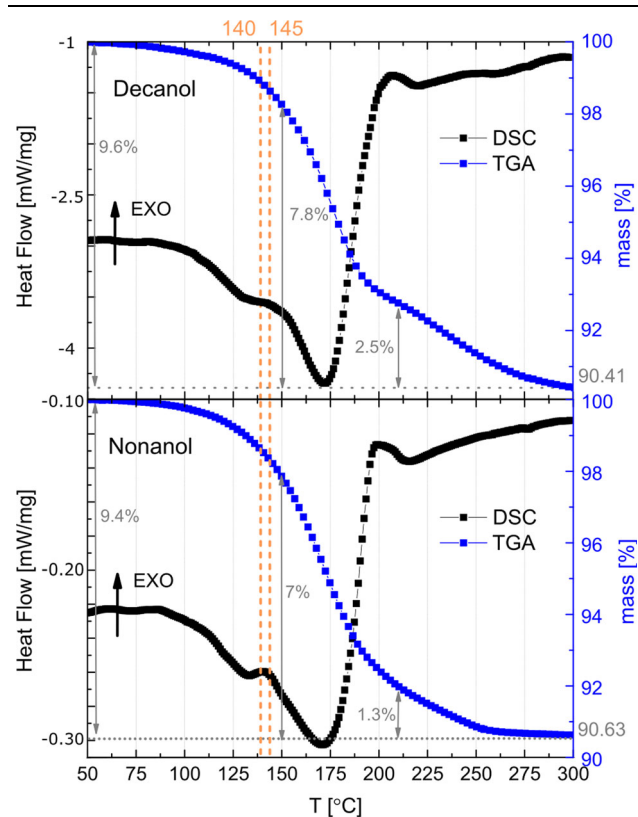


Fig. 5. TG-DSC curves obtained for the decanol- (top) and the nonanol-based pastes (bottom). The range of onset temperature of sintering is labelled in orange for both formulations.

We used DSC to detect eventual physical transformations of the material during sintering by measuring changes in the heat flow to the sample while heating. An endothermic heat flow was observed for both mixtures, starting at 80°C, peaking at 165°C, and ending at 200°C for the nonanol paste and at 217°C for the decanol formulation. For both samples, this endothermic profile was interrupted by a plateau between 140°C and 145°C.

The measured mass losses and endothermic peak are associated with the evaporation of the organic constituents of the mixtures. Interestingly, less than 25% of the organics in the pastes evaporate before the onset temperature of sintering (i.e. 141–144°C), meaning that most of the liquid phase is still present when neck formation takes place. Moreover, the plateau in the endothermic profile occurs exactly at the onset temperature of sintering for both mixtures. We believe this plateau results from the presence of an exothermic peak that overlays the endothermic process. This is typically observed during neck formation of NPs and is associated with the reduction of surface energy by atomic diffusion.^{18,22,39} Since the surface diffusion of Cu atoms would be hindered by the presence of amine-based molecules on the NPs surface, the passivation layer must be thermally desorbed from the surface before sintering starts.⁴⁰ Such interpretation provides further evidence of the key role of the passivation layer in defining the onset temperature of sintering. Because the NPs are passivated with the same molecules in both pastes, no difference in the temperature of the exothermic peak is observed.

The faster mass drop and endothermic reaction of the nonanol paste compared with decanol is due to the higher vapor pressure and lower boiling temperature of its carrier solvent. This difference is expected to affect the microstructural evolution of the sample during sintering.

Microstructural Evolution

We examined the evolution of the nano- and microstructures of the studied Cu pastes during sintering by means of SEM images and electrical measurements obtained from thin films sintered at different maximum temperatures in argon atmosphere (Fig. 6a and b).

SEM images show the average size of the microstructural domains at the given temperature of sintering (Fig. 6a). By definition, each of these domains is composed of many grains, as described by Lange et al.⁴¹

For both formulations, the samples sintered at 220°C showed a more extensive neck network between the domains than those sintered at 175°C. However, no significant changes in the microstructural domains were measured, with the average domain size being less than 200 nm. The increased necking was accompanied by a pronounced reduction in the electrical resistivity of

both mixtures as the temperature increased from 175°C to 220°C (Fig. 6b).

At 250°C, the nonanol mixture showed a dramatic growth of the domain size, which increased from 179 nm measured at 220°C to 457 nm. This growth

was not observed in the decanol sample until a temperature of 300°C, where an average size of 531 nm was reached. Moreover, a continuous decrease of the electrical resistivity was measured at increasing sintering temperatures, yielding

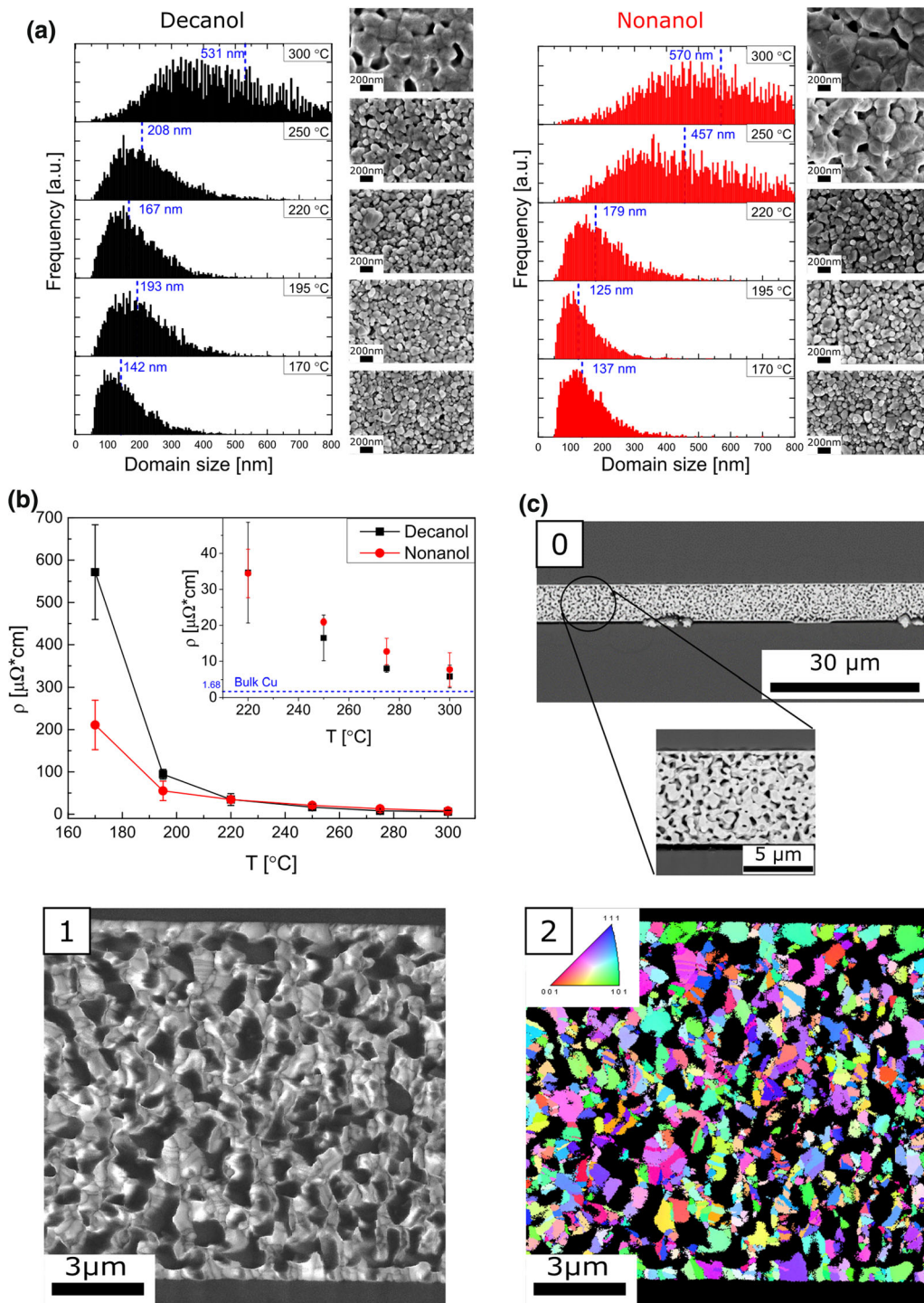


Fig. 6. (a) Domain size and SEM images obtained for samples of decanol and nonanol-based pastes as a function of the maximum sintering temperature. SEM; (b) Electrical resistivity of the samples as a function of maximum sintering temperature; (c) Nonanol paste layer sintered between a Cu-coated die and a silicon substrate: (0) Cross section SEM image; (1, 2) Orientation map from the same sample, where grains are depicted in colors that represent their crystallographic orientation (Color figure online).

values of $7.7 \pm 4.6 \mu\Omega \text{ cm}$ and $5.8 \pm 3.1 \mu\Omega \text{ cm}$ at 300°C for the nonanol and decanol mixtures, respectively. Maximal thermal conductivities of 238 W/m K and 269 W/m K were derived from these values for the nonanol and decanol pastes using the Wiedemann-Franz law.³⁵ This corresponds to about 60% of the thermal conductivity of bulk Cu.

Together with the dramatic growth of the domains, strong densification of the agglomerates occurred during the heating process. Interestingly, these growth and densification processes take place only above a certain temperature threshold, which is defined by the properties of the carrier solvent. Therefore, the maximum temperature needed to sinter the Cu paste correctly can be tuned by selecting the optimal carrier solvent. Once the threshold temperature is overcome, the carrier solvent has no significant impact on the final resistivity of the material. Indeed, the nonanol formulation can be fully sintered at 250°C , whereas 300°C must be reached to obtain a similar result with decanol.

Finally, we investigated the evolution of the nano- and microstructure of a Cu paste during sintering when constrained in the sandwich-type structure formed in the die attachment process. To this end, electron backscatter diffraction (EBSD) was performed on a nonanol paste sintered at 300°C between a Cu-coated Si die and a silicon substrate (Fig. 6c). SEM images showed a porosity of 22% in the sintered layer and an effective bonding of the sintered Cu on both the Cu metallization on the die and the silicon substrate (Fig. 6c). From the EBSD analysis an average grain size of 188 nm was recorded. The grains of the Cu metallization layer showed some preferred crystallographic orientation along the $\langle 101 \rangle$ direction, whereas no clear texture was detected in the grains of the sintered Cu. Moreover, the EBSD mapping revealed the formation of many twin boundaries within the copper grains.

The large grain size recorded with respect to the initial size distribution of the NPs (i.e. 10–60 nm) indicates that grain growth also takes place during heating of the Cu paste in the sandwich-like structure. This coarsening effect is well-known in ceramics^{42,43} and is attributed to the difference in curvature of small and large grains in the last stage of the sintering process. Such a curvature difference drives the transport of Cu atoms from smaller to larger particles, eventually reducing the density of grain boundaries in the system. The curved grain boundaries that drive coarsening are formed when the size ratio between the particles is greater than a critical value.⁴⁴ This coarsening mechanism also leads to the formation of the observed twin boundaries.⁴⁵ The interdiffusion between the sintered material and the metallization layer suggests that electrical, thermal and mechanical connections between the die and the substrate can be obtained by sintering the Cu pastes.

Die Attachment

To further evaluate the suitability of the proposed Cu pastes for die attachment, samples of decanol and nonanol pastes were sintered under glass dies with areas of 9 mm^2 , 25 mm^2 and 100 mm^2 . Optical and SEM imaging were then used to examine the eventual formation of macrovoids (area coverage $> 5000 \mu\text{m}^2$) and the sintering kinetics within different regions of the paste under the die (Fig. 7). Note that a pinkish-orange color developed upon sintering of the Cu NPs, in agreement with the results above and previous reports from the literature.⁴⁶

For the decanol formulation, an increase in macrovoid area fraction from 3% to 18% was recorded as the die area was increased from 9 mm^2 to 100 mm^2 . Such macrovoids appear in brown color in the central region of the sample, where the SEM analysis revealed a poor densification of the paste. By contrast, the nonanol mixture showed a stable macrovoid area fraction of about 5%, independent of the die size. With this solvent, an area of 100 mm^2 was uniformly sintered in all the regions under the die.

Our results show that the properties of the solvent are critical to achieve a successful attachment of large-area dies (i.e. $> 25 \text{ mm}^2$). The formation of macrovoids during sintering probably results from the constrained shrinkage of the paste during

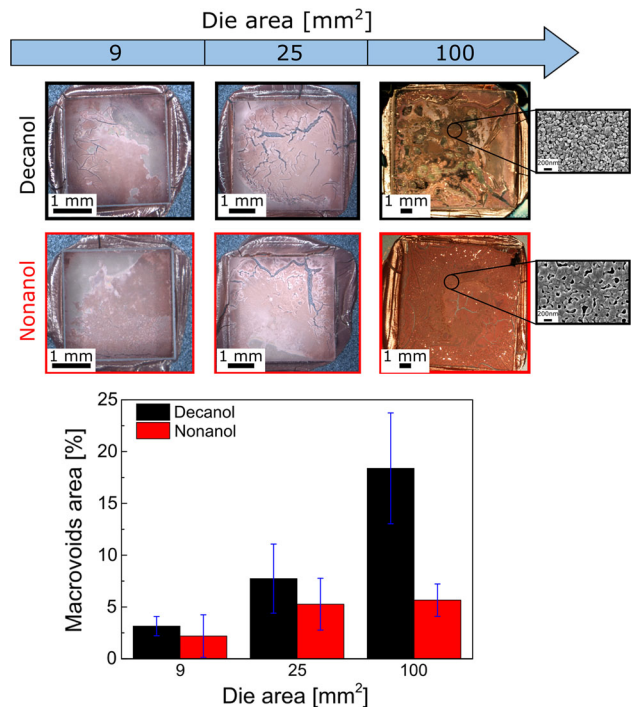


Fig. 7. (a) Optical images of pastes sintered under glass dies of different areas. The color difference between the images with a die area $\leq 25 \text{ mm}^2$ and those with a die area $> 25 \text{ mm}^2$ is due to the use of two different illumination sources. SEM images corresponding to specific regions under the die are shown; (b) Macrovoid area calculated from the optical images as a function of the die area.

evaporation of the carrier solvent. In fact, the sandwiched structure of the die attachment limits the interface area available for exchange between the solvent vapor and the atmosphere around the die. This condition is accentuated with increasing die area. Moreover, the exchange interface is further constrained by the formation of agglomerates at the onset temperature of sintering, which can trap solvent at the central region under a large die and thus locally hinder the densification of the material. To avoid this, it is crucial to evaporate as much solvent as possible before the agglomerates start to densify. Indeed, a high extent of sintering in every region under the die can be achieved by using carrier solvents with a low boiling point and high vapor pressure. Consequently, the nonanol paste formulation is preferred over decanol for the attachment of large dies.

CONCLUSIONS

Oxide-free Cu pastes with a lifespan in air of at least 30 min can be sintered in inert atmosphere without the need for a reducing agent, making them suitable for the cost-effective attachment of high-power devices in microelectronic applications. Using nonanol and decanol as carrier solvents, pastes sintered at a maximum temperature of 300°C in nitrogen led to Cu thin films with electrical resistivities on the same order of magnitude of bulk copper. For these pastes, a network of electrically conductive Cu NPs starts to form at a temperature between 141°C and 144°C, independent of the carrier solvent used. At this temperature, the amine-based passivation layer probably desorbs from the NPs surface, thus enabling the diffusion of the Cu atoms towards interparticle necks. The onset temperature of sintering for these pastes is therefore determined primarily by the choice of passivation layer. By contrast, the densification of the particle network is affected by the properties of the carrier solvent. This densification takes place at a temperature of 250°C for the nonanol paste and at 300°C for decanol formulation. Furthermore, only formulations based on a solvent with a low boiling point and a high vapor pressure, such as nonanol, can be uniformly sintered under die areas as high as 100 mm². The resulting attachment layer achieved high electrical and thermal connectivity, while keeping a low macrovoid area of approximately 5%. By understanding the effect of the different constituents on the sintering process of the Cu paste, it is possible to adjust the formulation to meet the maximum temperature and areal requirements of each specific application. Such versatility makes the proposed oxide-free Cu pastes an attractive electronic-packaging material in future die-attachment technology.

ACKNOWLEDGMENTS

The authors thank Kunze Karsten from the Scientific Center for Optical and Electron Microscopy to have performed the EBSD analysis, Francesco Pagani from EMPA for his help in the interpretation of impedance characterization, Ute Drechsler for her support with the electrode fabrications, Diana Davila Pineda for her support with the Raman analysis, Lilli-Marie Pavka for the copyediting of this manuscript, and Bruno Michel and Walter Riess for their continuous support. This project has been supported by the Swiss National Foundation, Project 200021_160189: “Controlled Drying of Colloidal Suspensions in Porous Structures for Neck-Based Interconnects.”

ELECTRONIC SUPPLEMENTARY MATERIAL

The online version of this article (<https://doi.org/10.1007/s11664-019-07452-8>) contains supplementary material, which is available to authorized users.

REFERENCES

1. J. Nelson, *The Physics of Solar Cells* (London: Imperial College Press, 2003).
2. Y. Mikamura, K. Hiratsuka, T. Tsuno, H. Michikoshi, S. Tanaka, T. Masuda, K. Wada, T. Horii, J. Genba, and T. Hiyoshi, *IEEE Trans. Electron Devices* 62, 382 (2015).
3. P. Neudeck, R. Okojie, and L. Chen, *Proc. IEEE* 90, 1065 (2002).
4. L. Lorenz, T. Erlbacher, O. Hilt, and K. Suganuma, *Woodhead Publishing Series in Electronic and Optical Materials* (Cambridge: Woodhead Publishing, 2018), pp. 3–53.
5. V.R. Manikam and K.Y. Cheong, *IEEE Trans. Comp. Packag. Manuf. Technol.* 1, 457 (2011).
6. K. Suganuma, *Woodhead Publishing Series in Electronic and Optical Materials* (Cambridge: Woodhead Publishing, 2018), pp. 57–80.
7. European Commission. *Directive 2011/65/EU of The European Parliament and of the Council of 8 June 2011—ROHS*, vol. 54, pp. 88–110 (2011).
8. K. Suganuma, S.J. Kim, and K.S. Kim, *JOM* 61, 64–71 (2009).
9. J.G. Bai, J. Yin, Z. Zhang, G.Q. Lu, and J.D. van Wyk, *IEEE Trans. Adv. Packag.* 30, 506–510 (2007).
10. T. Wang, X. Chen, G.Q. Lu, and G.Y. Lei, *J. Electron. Mater.* 36, 1333 (2007).
11. R. Khazaka, L. Mendizabal, and D. Henry, *J. Electron. Mater.* 43, 2459 (2014).
12. M. Gutierrez, N. Wang, M.K. Samani, L. Ye, and J. Liu, in *IMAPS Nordic Conference on Microelectronics Packaging (NordPac)*, p. 151 (2017).
13. S. Magdassi, M. Grouchko, and A. Kamyshny, *Materials (Basel)* 3, 4626 (2010).
14. W. Li, L. Li, Y. Gao, D. Hu, C.F. Li, H. Zhang, J. Jiu, S. Nagao, and K. Suganuma, *J. Alloys Compd.* 732, 240 (2018).
15. S. Sun, Q. Guo, H. Chen, M. Li, and C. Wang, *Microelectron. Reliab.* 80, 2018 (2017).

16. L. Del Carro, J. Zuercher, S. Gerke, T. Wildsmith, G. Ramos, and T. Brunschwiler, in *2017 IEEE 67th Electronic Components and Technology Conference (ECTC)*. IEEE, p. 961 (2017).
17. J. Zurcher, L. Del Carro, G. Schlottig, D.N. Wright, A.S.B. Vardoy, M.M.V. Taklo, T. Mills, U. Zschenderlein, B. Wunderle, and T. Brunschwiler, in *IEEE 66th Electronic Components and Technology Conference (ECTC)*, p. 343 (2016).
18. J. Liu, H. Chen, H. Ji, and M. Li, *ACS Appl. Mater. Interfaces* 8, 33289 (2016).
19. A.A. Zinn, R.M. Stoltenberg, J. Chang, Y.L. Tseng, and S.M. Clark, in *16th International Conference on Nanotechnology-IEEE NANO*, p. 367 (2016).
20. B.H. Lee, M.Z. Ng, A.A. Zinn, and C.L. Gan, in *Proceedings of the International Symposium on the Physical and Failure Analysis of Integrated Circuits, IPFA*, p. 102 (2015).
21. A.A. Zinn, R.M. Stoltenberg, J. Chang, Y.L. Tseng, S.M. Clark, and D.A.A. Cullen, in *2016 IEEE 18th Electronics Packaging Technology Conference (EPTC)* p 1 (2016).
22. M. Kanzaki, Y. Kawaguchi, H. Kawasaki, *ACS Appl. Mater. Interfaces* 9, 20852 (2017).
23. B.H. Lee, M.Z. Ng, A.A. Zinn, and C.L. Gan, in *Proceedings of the Electronic Packaging Technology Conference, EPTC* (2016).
24. A. Zinn, Lead Solder-Free Electronic (2009). <https://patent.google.com/patent/US8105414B2/en>.
25. K. Schnabl, L. Wentlent, K. Mootoo, S. Khasawneh, A.A. Zinn, J. Beddow, E. Hauptfleisch, D. Blass, and P. Borgesen, *J. Electron. Mater.* 43, 4515 (2014).
26. A.A. Zinn, P.P. Lu, Nanoparticle Composition and Methods of Making the Same (2013). <https://patents.google.com/patent/US8486305B2/en>.
27. A.A. Zinn, Copper Nanoparticle Application Process for Low Temperature Printable, Flexible/Conformal Electronics and Antennas (2015). <https://patents.google.com/patent/US9072185B2/en>.
28. Y. Deng, A.D. Handoko, Y. Du, S. Xi, and B.S. Yeo, *ACS Catal.* 6, 2473 (2016).
29. A.D. Handoko, S. Deng, Y. Deng, A.W.F. Cheng, K.W. Chan, H.R. Tan, Y. Pan, E.S. Tok, C.H. Sow, and B.S. Yeo, *Catal. Sci. Technol.* 6, 269 (2016).
30. A. Soon, M. Todorova, B. Delley, and C. Stampfl, *Phys. Rev. B* 75, 125420 (2007).
31. L. De Los Santos Valladares, D.H. Salinas, A.B. Dominguez, D.A. Najarro, S.I. Khondaker, T. Mitrelias, C.H.W. Barnes, J.A. Aguiar, and Y. Majima, *Thin Solid Films* 520, 6368 (2012).
32. Z. Fang, *Sintering of Advanced Materials* (Woodhead Publishing Limited, 2010).
33. J. Habasaki, C. Leon, and K.L. Ngai, *Dynamics of Glassy, Crystalline and Liquid Ionic Conductors*, vol. 132 (Switzerland: Springer International Publishing, 2017).
34. A.J. Bard and L.R. Faulkner, *Electrochemical Methods Fundamentals and Applications*, 2nd ed. (New York: Wiley, 2001).
35. J.M. Montes, J.A. Rodríguez, and E.J. Herrera, *Powder Metall.* 46, 251 (2003).
36. E.J. De Souza, M. Brinkmann, C. Mohrdieck, and E. Arzt, *Langmuir* 24, 8813 (2008).
37. J. Zürcher, B.R. Burg, L. Del Carro, A.R. Studart, and T. Brunschwiler, *Transp. Porous Media* 125, 173 (2018).
38. R. Stadler, L. Del Carro, J. Zurcher, G. Schlottig, A.R. Studart, and T. Brunschwiler, in *2017 16th IEEE Intersociety Conference on Thermal and Thermomechanical Phenomena in Electronic Systems (ITherm)*. IEEE, p. 167 (2017).
39. T. Sugiyama, M. Kanzaki, R. Arakawa, and H. Kawasaki, *J. Mater. Sci. Mater. Electron.* 27, 7540 (2016).
40. C. Kim, G. Lee, C. Rhee, and M. Lee, *Nanoscale* 7, 6627 (2015).
41. F.F. Lange, *J. Am. Ceram. Soc.* 67, 83 (1984).
42. Z.Z. Fang, H. Wang, X. Wang, and V. Kumar, *Ceram. Trans.* 209, 389 (2010).
43. J.R. Groza, *Nanostructured Mater.* 12, 987 (1999).
44. R.H.R. Castro, *Sintering: Mechanisms of Conversion Nanodensification and Field Assisted Processes* (Berlin, Heidelberg: Springer-Verlag, 2013).
45. S.K. Volkman, S. Yin, T. Bakhishev, K. Puntambekar, V. Subramanian, and M.F. Toney, *Chem. Mater.* 23, 4634 (2011).
46. M. Zenou, O. Ermak, A. Saar, and Z. Kotler, *J. Phys. D Appl. Phys.* 47, 025501 (2014).

Publisher's Note Springer Nature remains neutral with regard to jurisdictional claims in published maps and institutional affiliations.